Plasma Sources Sci. Technol. **20** (2011) 045008 (14pp) doi:10.1088/0963-0252/20/4/045008

Electron heating and the electrical asymmetry effect in dual-frequency capacitive CF_4 discharges

J Schulze[1,2], A Derzsi[1] and Z Donkó[1]

[1] Research Institute for Solid State Physics and Optics of the Hungarian Academy of Sciences, Konkoly-Thege Miklós str. 29-33, H 1121 Budapest, Hungary
[2] Institute for Plasma and Atomic Physics, Ruhr-University Bochum, Universitätsstr. 150, 44780 Bochum, Germany

E-mail: fjschulze@hotmail.com

Received 15 March 2011, in final form 18 April 2011
Published 3 June 2011
Online at stacks.iop.org/PSST/20/045008

Abstract
The electron heating and the electrical asymmetry effect (EAE) in electronegative dual-frequency capacitive CF_4 discharges are investigated by particle-in-cell simulations and analytical modeling. One electrode is driven at 13.56 and 27.12 MHz with fixed but adjustable phase shift, θ, between the driving harmonics. First, the electron heating and ionization rates are studied, space and time resolved, for different phase shifts and pressures. The results are compared with those obtained for an electropositive gas (argon). In contrast to classical α- or γ-mode operation, we observe the electron heating and ionization rates to be high inside the bulk. This bulk heating mode is a consequence of the high electronegativity of CF_4 discharges, where the conductivity in the bulk is low due to the low density of electrons. Thus, a high electric field builds up to drive the RF current through the bulk causing a high electron mean energy and ionization rate in the discharge center. Second, we investigate the consequences of the bulk heating on the EAE. We focus on the electrical generation of a dc self-bias as a function of θ and the quality of the separate control of the ion mean energy and flux at the electrodes by tuning θ. Compared with argon discharges the high voltage drop across the plasma bulk and the specific ionization dynamics affect the bias generation and the separate control of ion properties. These effects are described and explained by an analytical model.

(Some figures in this article are in colour only in the electronic version)

1. Introduction

Capacitively coupled radio frequency (CCRF) discharges are frequently used for applications such as plasma etching or plasma enhanced chemical vapor deposition (PECVD) processes in the frame of semiconductor manufacturing and the creation of biocompatible surfaces [1, 2]. These applications usually require complex mixtures of reactive, often electronegative gases such as CF_4, which is widely used to etch silicon and silicon dioxide [1]. Generally, these processes are sensitive to the energy and the flux of ions bombarding the substrate. Thus, a detailed understanding of electron heating and methods to control the ion mean energy, $\langle E_i \rangle$, at the electrodes separately from the ion flux, Γ_i, in reactive electronegative gases is most important.

Electron heating in electropositive CCRF discharges has been studied intensively using experiments, simulations and models [3–16]. It was found that these discharges are usually operated in either α-mode (low pressure and/or voltages) or γ-mode (high pressures and/or voltages), where the electron heating and ionization are dominated by sheath expansion heating and secondary electrons, respectively [17–19]. In α-mode also field reversals during sheath collapse can cause significant electron heating and ionization [18, 20–23]. In both modes, the ionization and heating rates as well as the mean electron energy typically peak around the sheath edges and are low inside the bulk.

Previous investigations of CF_4 discharges have demonstrated this gas to be reactive and electronegative [24–40]. In contrast to electropositive discharges a different heating mode was observed in time averaged results of simulation studies of CF_4 discharges. This mode is characterized by a high ionization and electron mean energy in the plasma bulk [29–31]. A similar bulk heating mode has also been observed in other strongly electronegative gases such as SiH_4 [41] and SF_6 [42], where a strong electric field in the bulk was found to accelerate electrons to high energies causing significant ionization in the discharge center. Proshina *et al* [30] and Denpoh *et al* [31] investigated the transition of CF_4 discharges from classical electron heating into the bulk heating mode and observed it to depend on the discharge pressure and driving voltage. In order to obtain a detailed understanding of the bulk heating and the transition from classical heating into the bulk heating mode in CF_4 discharges, time resolved investigations of the electron heating rate and ionization dynamics are clearly required.

In order to realize separate control of $\langle E_i \rangle$ and Γ_i at the electrodes, hybrid plasma sources (RF-DC [43, 44], capacitive-helicon [45–47], capacitive-inductive [46, 48, 49]) or dual-frequency (df) capacitive RF discharges [50–54] can be used. In classical df discharges operated at substantially different frequencies, e.g. 2 MHz and 27 MHz, $\langle E_i \rangle$ and Γ_i are controlled by the low frequency (lf) and high frequency (hf) voltage amplitude, ϕ_{lf} and ϕ_{hf}, respectively. However, studies of the electron heating in such discharges have revealed a strong coupling between both frequencies that limits the quality of this separate control [55–61], which is additionally reduced by the effect of secondary electrons [61–63].

In contrast to such classical df discharges, the quality of the separate control of ion properties was found to be significantly better in discharges driven by a fundamental frequency and its second harmonic with fixed, but adjustable phase shift, θ, between the driving harmonics. In such discharges, a dc self-bias, η, is generated electrically as a function of θ via the electrical asymmetry effect (EAE) [64–76] and $\langle E_i \rangle$ can be controlled separately from Γ_i by adjusting θ, avoiding any frequency coupling and suppressing negative effects of secondary electrons [63]. Previous investigations of the EAE have mostly been limited to fundamental studies in argon, except those of Hou *et al* in pure oxygen [74], where the EAE was found to work similarly compared with electropositive discharges. More detailed studies in other gases relevant for applications are therefore necessary.

Here, we investigate electrically asymmetric df discharges in CF_4 by particle-in-cell simulations complemented with Monte Carlo treatment of collision processes (PIC/MCC) at different pressures and values of θ. First, we study the electron heating and ionization dynamics. At low pressures, we find α-mode heating to be dominant, while the discharge is operated in the bulk heating mode at high pressures. We investigate the bulk heating mode in more detail by studying plasma parameters such as the electron heating and ionization rates, space and time resolved within the hf period. We find the bulk heating to be caused by a high reduced electric field, E/n, in the discharge center and a high voltage drop across the plasma bulk. This, in turn, is caused by the strong electronegativity of the discharge, i.e. the low number of electrons and low conductivity inside the bulk that require a strong electric field to drive the RF current through the discharge center. We compare our results with those derived from simulations of argon discharges operated in α-mode under identical conditions and find the ionization dynamics to work differently in CF_4. Second, we study the consequences of the bulk heating mode on the EAE with focus on the separate control of $\langle E_i \rangle$ and Γ_i. Again, we compare our results with those obtained for argon to point out differences to electropositive discharges. We find the electrical generation of the dc self-bias to be affected by the high voltage drop across the plasma bulk and the specific ionization dynamics in the bulk heating mode. These effects are described and explained by an analytical model.

The paper is structured in the following way: in the second section, the PIC/MCC simulation is described including all collision processes taken into account. Then, the analytical model of the EAE used to describe the electrical generation of a dc self-bias as a function of θ is introduced. In the fourth section, the simulation results are presented. This section is divided into two parts: in the first part, the electron heating and ionization dynamics in electrically asymmetric df discharges are investigated with focus on the bulk heating in CF_4. The results are compared with electropositive argon discharges. In the second part, the consequences of the bulk heating on the EAE and the separate control of the mean ion energy and flux at the electrodes are discussed and understood by an analytical model. Finally, conclusions are drawn in section five.

2. Simulation method

We use a one-dimensional (1D3V) bounded PIC/MCC code to investigate electron heating and the EAE in geometrically symmetric df discharges in pure argon and pure CF_4, respectively. The following voltage waveform, $\tilde{\phi}(t)$, is applied to one electrode, while the other electrode is grounded:

$$\tilde{\phi}(t) = \phi_{lf} \cos(2\pi f t + \theta) + \phi_{hf} \cos(4\pi f t). \quad (1)$$

Here, t is time and $f = 13.56\,\text{MHz}$. The electrodes are assumed to be plane parallel and separated by a distance $d = 2.5\,\text{cm}$. The gas temperature is 350 K. Ion induced emission of secondary electrons is taken into account ($\gamma = 0.1$). Electrons hitting the electrode are reflected with a probability of 20% [77]. Simulations are performed at 30 and 50 Pa for different values of θ between 0° and 90° (in 10° steps). Equal voltage amplitudes of both driving harmonics are used, i.e. $\phi_{lf} = \phi_{hf} = 100\,\text{V}$ at 30 Pa and $\phi_{lf} = \phi_{hf} = 50\,\text{V}$ at 50 Pa. Thus, identical conditions in argon and CF_4 discharges are investigated at each neutral gas pressure.

The dc self-bias, η, is determined iteratively in the following way: at the initialization of the simulation a bias of 0 V is set. After executing the simulation for a given number of hf cycles (typically 50), the fluxes of the positively and negatively charged particles to each of the two electrodes are evaluated. Depending on the balance of these fluxes, the bias is changed by a small value. This procedure is continued until the bias reaches a converged value and the charged particle fluxes to each of the two electrodes balance.

Table 1. List of electron–CF_4 collisions considered in the model. E_0 is the energy threshold in eV.

Collision type	Product	E_0
Elastic momentum transfer		0
Vibrational excitation		0.108
Vibrational excitation		0.168
Vibrational excitation		0.077
Electronic excitation	CF_4^*	7.54
Dissociative ionization	CF_3^{++}	41
Dissociative ionization	CF_3^+	16
Dissociative ionization	CF_2^{++}	42
Dissociative ionization	CF_2^+	21
Dissociative ionization	CF^+	26
Dissociative ionization	C^+	34
Dissociative ionization	F^+	34
Attachment	F^-	0
Attachment	CF_3^-	0
Neutral dissociation	CF_3	12
Neutral dissociation	CF_2	17
Neutral dissociation	CF	18

For the simulations in pure argon, the cross sections for electron–neutral and ion–neutral collisions are taken from Phelps and Petrović [78–80]. For the argon ions, elastic collisions with the neutral gas atoms are divided into an isotropic and a backward part. Details of the code for argon can be found elsewhere [57, 63, 66].

For the simulations in CF_4, four types of charged species, i.e. CF_3^+, CF_3^-, F^- ions and electrons, are traced in the code. These charged particle species were found to be the dominant species by earlier studies [24–30]. Additional electron-impact collision processes resulting in the formation of other types of charged species are assumed to affect only the electron kinetics, but their products are not traced in the simulation. The electron–neutral collision processes taken into account are listed in table 1. The cross sections for e^-–CF_4 collisions are taken from [81], with the exception of electron attachment processes (producing CF_3^- and F^- ions), which are taken from Bonham [82].

The ion–molecule reactions in CF_4 involve numerous channels and there is a large number of reaction processes, which could be taken into account in a simulation [24, 29, 83]. Here, we consider a set of collision processes including reactive as well as elastic collisions of different ions with CF_4 molecules. These processes are listed in table 2. The treatment of ion–neutral collisions is based on previous work [25, 83, 84].

Recombination processes between positive and negative ions as well as between electrons and CF_3^+ ions are simulated according to the procedure of Nanbu and Denpoh [85]. The rate of electron–CF_3^+ recombination is taken from Denpoh and Nanbu [31]. Different values for the ion–ion recombination rate coefficients ranging from 1×10^{-13} m^3 s^{-1} to 5.5×10^{-13} m^3 s^{-1} can be found in the literature [24, 29, 30, 86, 87]. We use the value provided by Rauf and Kushner [86], 1×10^{-13} m^3 s^{-1}, in order to ensure consistency with our previous simulation studies of CF_4 discharges [28]. However, we perform simulations for distinct sets of discharge conditions using also the higher recombination rate of 5.5×10^{-13} m^3 s^{-1} [30] to check the sensitivity of our results on this input parameter. The recombination processes and rates taken into account in the simulation are listed in table 3.

Table 2. Ion–CF_4 collisions considered in the simulation. E_0 is the energy threshold in eV.

Projectile	Reaction	E_0
CF_3^+	$CF_3^+ + CF_4 \rightarrow CF_2^+ + CF_4 + F$	5.843
CF_3^+	$CF_3^+ + CF_4 \rightarrow CF_3^+ + CF_3 + F$	5.621
CF_3^+	$CF_3^+ + CF_4 \rightarrow CF_3^+ + CF_4$	0
CF_3^-	$CF_3^- + CF_4 \rightarrow CF_4 + CF_3 + e^-$	1.871
CF_3^-	$CF_3^- + CF_4 \rightarrow CF_3^- + CF_3 + F$	5.621
CF_3^-	$CF_3^- + CF_4 \rightarrow CF_2 + CF_4 + F^-$	1.927
CF_3^-	$CF_3^- + CF_4 \rightarrow CF_3^- + CF_4$	0
F^-	$F^- + CF_4 \rightarrow CF_4 + F + e^-$	3.521
F^-	$F^- + CF_4 \rightarrow CF_3 + F^- + F$	5.621
F^-	$F^- + CF_4 \rightarrow F^- + CF_4$	0

Table 3. Recombination processes considered in the simulation. The ion and electron temperatures, T_i and T_e, respectively, are given in eV. The ion–ion recombination rates in parentheses correspond to the maximum values found in the literature, which are used for some distinct sets of discharge conditions to test the sensitivity of our results on this parameter.

Reaction	Rate coefficient (m^3 s^{-1})
$CF_3^+ + e^-$	$3.95 \times 10^{-15} T_i^{-1} T_e^{-0.5}$
$CF_3^+ + F^-$	1×10^{-13} (5.5×10^{-13})
$CF_3^+ + CF_3^-$	1×10^{-13} (5.5×10^{-13})

The processes listed in tables 1–3 are believed to be the dominant reactions influencing the electron kinetics and the charged particle balance for the major ionic species. However, it has to be noted that the chemistry considered here is largely simplified compared with that taking place in an experimental plasma reactor. We neglect a number of ionic species created by dissociative ionization, as well as all the neutral radicals and all their reactions taking place at the walls. Nonetheless, we expect our model to capture the basic features of electrically asymmetric CF_4 discharges and trust that the prominent effects discussed here will be confirmed in forthcoming experiments.

3. The analytical model of the EAE

The analytical model of the EAE has been developed by Czarnetzki *et al* [65, 76]. Here, only a short introduction of the model is presented and its analytical expression for the dc self-bias, η, is derived, which is later used to model the EAE in CF_4 discharges. The model is based on the voltage balance of CCRF discharges:

$$\tilde{\phi}(t) + \eta = \phi_{sp}(t) + \phi_{sg}(t) + \phi_b(t). \quad (2)$$

Here, $\tilde{\phi}(t)$ is the applied voltage waveform as a function of time (equation (1)), $\phi_{sp}(t)$, $\phi_{sg}(t)$ are the voltage drops across the sheath at the powered and grounded electrodes, respectively, and $\phi_b(t)$ is the bulk voltage at a given time within the RF period. Combining equation (2) at the time of maximum and minimum applied voltages yields an analytical expression for the dc self-bias normalized by the amplitude of the driving

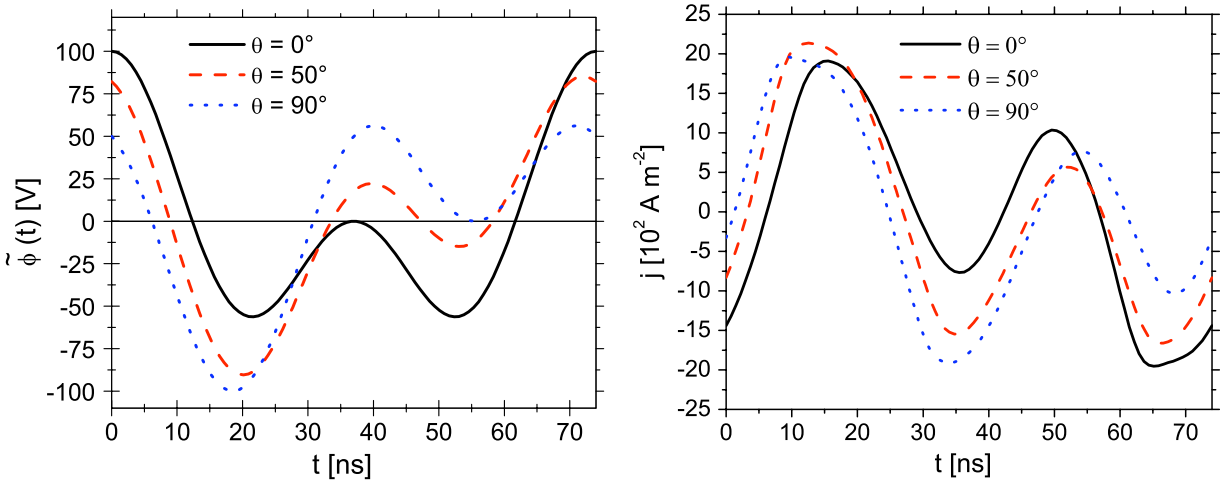

Figure 1. Driving voltage waveform (left) and electron conduction current density in the discharge center (right) as a function of time within one lf period for different values of θ in an electrically asymmetric df CF_4 discharge at 50 Pa, $\phi_{lf} = \phi_{hf} = 50$ V.

voltage waveform, $\phi_{lf} + \phi_{hf}$ [65, 76]:

$$\bar{\eta} = \frac{1}{\phi_{lf} + \phi_{hf}} \left(-\frac{\tilde{\phi}_{max} + \varepsilon\tilde{\phi}_{min}}{1+\varepsilon} + \frac{\phi^{f}_{sp} + \varepsilon\phi^{f}_{sg}}{1+\varepsilon} + \frac{\phi^{b}_{max} + \varepsilon\phi^{b}_{min}}{1+\varepsilon} \right). \tag{3}$$

Here, $\bar{\eta}$ is the normalized dc self-bias, $\tilde{\phi}_{max}$, $\tilde{\phi}_{min}$ are the maximum and minimum of the driving voltage waveforms, ϕ^{f}_{sp}, ϕ^{f}_{sg} are the floating potentials at the powered and grounded electrodes, and ϕ^{b}_{max}, ϕ^{b}_{min} are the voltage drops across the plasma bulk at the time of maximum and minimum applied voltages, respectively. Note that $\phi^{f}_{sp}, \phi^{b}_{min} < 0$ V, whereas $\phi^{f}_{sg}, \phi^{b}_{max} > 0$ V. ε is the symmetry parameter:

$$\varepsilon = \left| \frac{\hat{\phi}_{sg}}{\hat{\phi}_{sp}} \right| = \left(\frac{A_p}{A_g} \right)^2 \frac{\bar{n}_{sp}}{\bar{n}_{sg}} \left(\frac{Q_{mg}}{Q_{mp}} \right)^2 \frac{I_{sg}}{I_{sp}}. \tag{4}$$

Here, $|\hat{\phi}_{sp}|$, $\hat{\phi}_{sg}$ are the maximum voltage drops across the sheath at the powered and grounded electrode ($\hat{\phi}_{sp} < 0$ V, $\hat{\phi}_{sg} > 0$ V). A_p, A_g are the surface areas of the powered and grounded electrodes (here: $A_p = A_g$), Q_{mp}, Q_{mg} are the maximum uncompensated charges in each sheath, and $\bar{n}_{sp}$, $\bar{n}_{sg}$ are the mean effective charge densities in the respective sheath:

$$\bar{n}_{sp,sg} = \frac{\int_0^{\hat{s}_{p,g}} [n_{CF_3^+}(x) - n_{F^-}(x) - n_{CF_3^-}(x)]\,dx}{\hat{s}_{p,g}}, \tag{5}$$

where x is the distance from the respective electrode and $n_{CF_3^+}(x)$, $n_{F^-}(x)$, $n_{CF_3^-}(x)$ are the space-dependent densities of CF_3^+, F^- and CF_3^- ions in the sheath. $\hat{s}_{p,g}$ is the maximum of the time-dependent sheath width at the powered and grounded electrode, $s_{p,g}(t)$, calculated according to Brinkmann [88]:

$$\int_0^{s_{p,g}(t)} n_e(x,t)\,dx = \int_{s_{p,g}(t)}^{d/2} [n_{CF_3^+}(x) - n_{F^-}(x) - n_{CF_3^-}(x) - n_e(x,t)]\,dx. \tag{6}$$

Here d is the electrode gap. In equation (4) I_{sp} and I_{sg} are the sheath integrals for the powered and grounded electrode sheath, respectively:

$$I_{sp,sg} = 2\int_0^1 p_{s_{p,g}}(\xi_{p,g})\xi_{p,g}\,d\xi_{p,g}, \tag{7}$$

with $\xi_{p,g} = x/\hat{s}_{p,g}$ and $p_{s_{p,g}}(\xi_{p,g}) = [n_{CF_3^+}(x) - n_{F^-}(x) - n_{CF_3^-}(x)]/\bar{n}_{sp,sg}$. Generally, $1 \leqslant I_{sp,sg} \leqslant 2$ depending on the ion density profiles in the respective sheath (typically $I_{sg}/I_{sp} \approx 1$, [65]).

4. Results

4.1. Electron heating in electrically asymmetric df CF_4 discharges

We investigate discharges driven by a voltage waveform according to equation (1) in pure CF_4 at 30 Pa ($\phi_{lf} = \phi_{hf} = 100$ V) and 50 Pa ($\phi_{lf} = \phi_{hf} = 50$ V) for different phase shifts between the driving harmonics of $\theta = 0°, 50°, 90°$. The results are compared with electropositive argon discharges at 50 Pa ($\phi_{lf} = \phi_{hf} = 50$ V). Figure 1 shows the driving voltage waveform (left plot) and the electron conduction current density in the discharge center (right plot) for different values of θ in a CF_4 discharge operated at 50 Pa as an example. The main results of our simulations are shown in figure 2 (charged particle density profiles), figure 3 (electron heating rate) and figure 4 (ionization rate, generation of Ar^+/CF_3^+). In each plot, the first row shows simulation results for argon discharges at 50 Pa, whereas the second and third rows correspond to discharges operated in CF_4 at 30 Pa and 50 Pa, respectively. Each column contains results for a particular value of θ (first column: $\theta = 0°$, second column: $\theta = 50°$, third column: $\theta = 90°$). First, we concentrate on the analysis of the data at $\theta = 0°$ to study basic features of the electron heating and ionization dynamics in CF_4 as well as differences to electropositive discharges. Second, we discuss the results for other values of θ.

For $\theta = 0°$, we observe time averaged charged particle density profiles typical for electropositive argon and electronegative CF_4 discharges (figure 2, [24–30]). The CF_4 discharges (second and third rows) are strongly

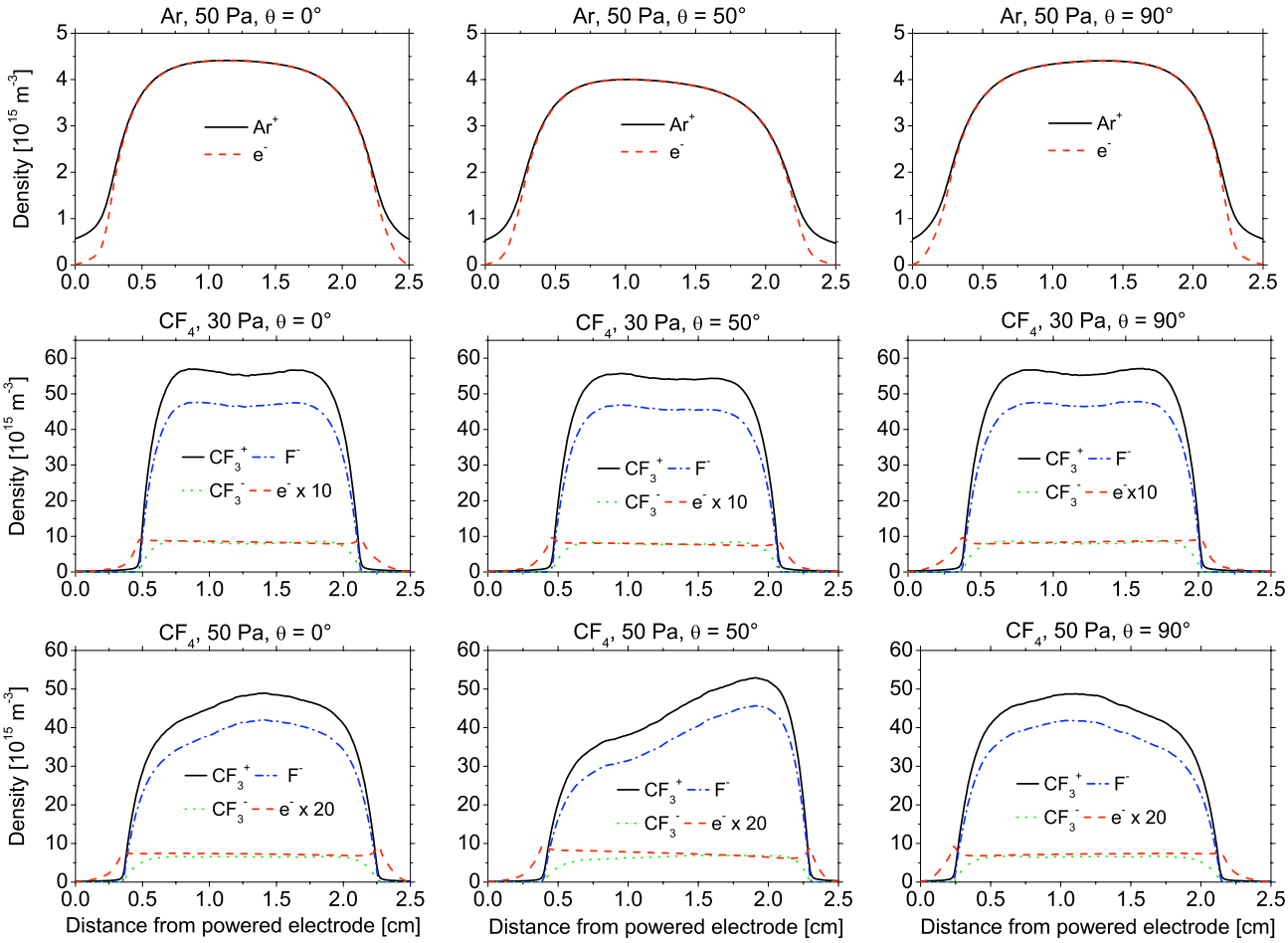

Figure 2. Time averaged charged particle densities in df discharges operated at 13.56 MHz + 27.12 MHz for different values of θ. First row: Ar, 50 Pa, $\phi_{lf} = \phi_{hf} = 50$ V. Second row: CF_4, 30 Pa, $\phi_{lf} = \phi_{hf} = 100$ V. Third row: CF_4, 50 Pa, $\phi_{lf} = \phi_{hf} = 50$ V.

electronegative, i.e. the electron density is significantly lower than the negative ion density. The electronegativity increases as a function of pressure due to the enhanced electron attachment at higher pressures. The dominant negative ion species is F^-, whose density is several times higher compared with CF_3^-. The negative ions are confined to the electronegative central region of the discharge, whereas the sheath regions adjacent to both electrodes are electropositive. At the transition point between the electronegative core and electropositive edge region a local maximum of the electron density is observed [24–30]. For $\theta = 0°$, the density profiles are approximately symmetric with respect to the discharge center.

The spatio-temporal distribution of the electron heating rate (figure 3) in electropositive argon discharges is dominated by sheath expansion heating. There is no significant heating in the plasma bulk, since the electric field in the discharge center is low, such as shown in figure 5. This, in turn, is caused by the high electron density in the discharge center, which leads to a high bulk conductivity, σ. Thus, only a low electric field, E, is required to drive a given RF current, j, through the plasma bulk:

$$j = \sigma E \qquad \text{with } \sigma = \frac{\bar{n}_b e^2}{m_e \nu_m}. \tag{8}$$

Here $\bar{n}_b$ is the effective electron density in the bulk, e is the elementary charge, m_e is the electron mass and ν_m is the electron–neutral elastic collision frequency.

The top plot of figure 5 shows the profile of the reduced electric field at the time of maximum electron heating at $\theta = 0°$ for the different discharge conditions investigated here. For argon (black solid line), the reduced electric field in the bulk is approximately 25 Td at this time ($t \approx 14$ ns). According to electron swarm studies [89, 90], this value is too low to cause significant ionization. Figure 6 shows the spatio-temporal distribution of the mean electron energy for $\theta = 0°$. In argon, the mean electron energy is low in the bulk and only slightly time modulated due to the propagation of highly energetic electron beams into the bulk generated by the expanding sheaths [19]. The propagation of these beams is indicated by the arrows in the top plot of figure 6. The modulation of the mean electron energy is small, since the number of highly energetic beam electrons is small compared with the number of cold bulk electrons [19] and the mean electron energy is calculated by averaging over all electrons at a given position and time. Inside the sheaths (gray areas in figure 6) the mean electron energy is high, since the only electrons present in this region are highly energetic secondary electrons. The spatio-temporal ionization rate in argon discharges is dominated by sheath expansion heating (figure 4), i.e. the discharge is operated in α-mode. The observed ionization dynamics in electrically asymmetric df discharges operated in α-mode has been described and understood by an analytical model based on the generation of highly energetic

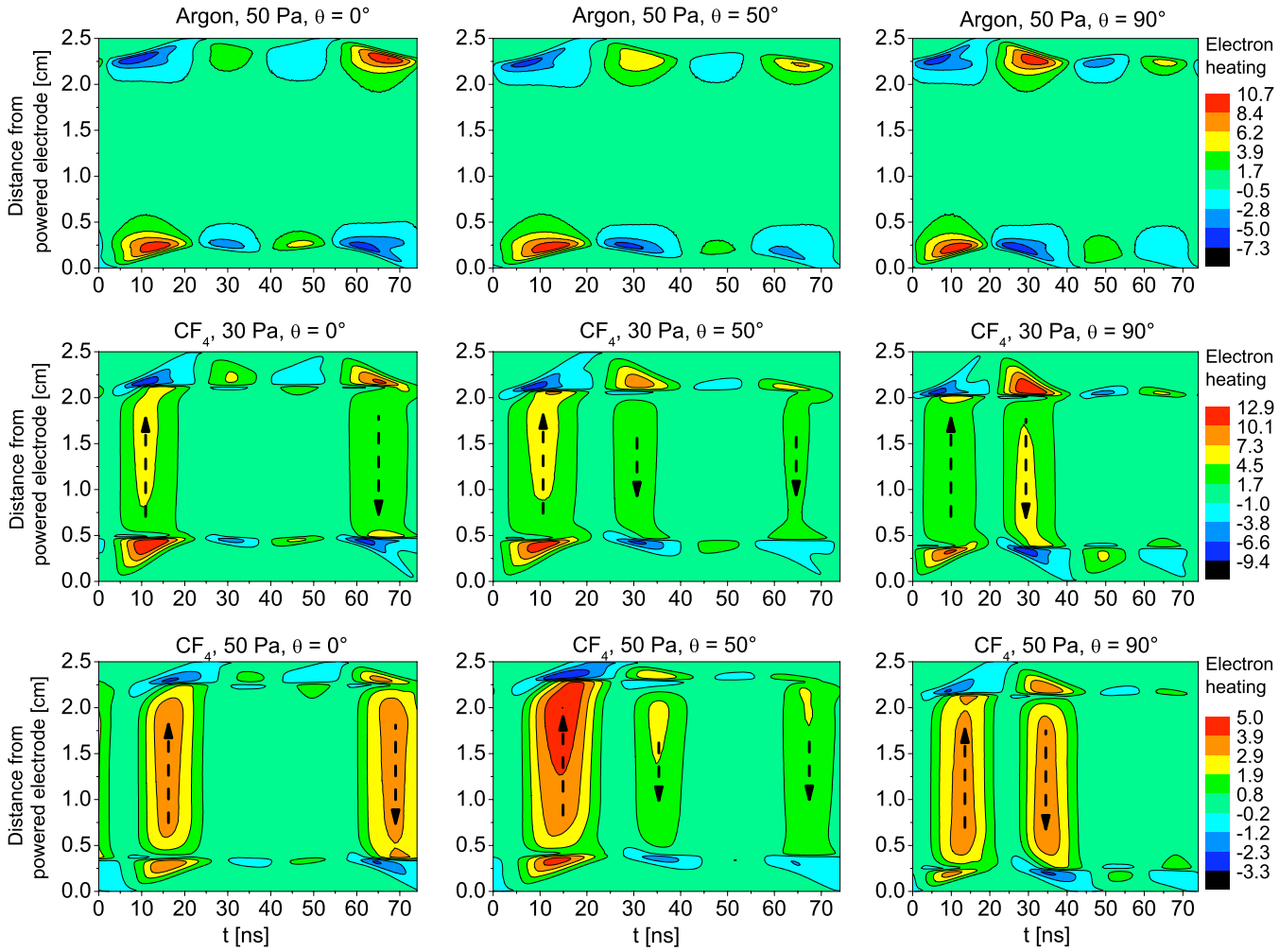

Figure 3. Spatio-temporal distribution of the electron heating rate in df discharges operated at 13.56 MHz + 27.12 MHz for different values of θ. First row: Ar, 50 Pa, $\phi_{lf} = \phi_{hf} = 50$ V. Second row: CF_4, 30 Pa, $\phi_{lf} = \phi_{hf} = 100$ V. Third row: CF_4, 50 Pa, $\phi_{lf} = \phi_{hf} = 50$ V. The color scale is given in 10^4 W m^{-3} and is the same for all plots in one row. The arrows indicate the momentary direction and relative amplitude of the electron acceleration (reversed direction of the electric field) in the plasma bulk.

electron beams by the expanding sheaths [72]. Generally, the maxima of the electron heating and ionization rates do not occur at the same time, but the ionization rate peaks a few nanoseconds later than the electron heating rate. This delay is caused by the time required to accelerate electrons above the threshold energy for ionization and to undergo an ionizing collision.

In CF_4 discharges, the electron heating and ionization dynamics work differently. Due to the high electronegativity and low electron density in the discharge center, the bulk conductivity is low and a high electric field in the discharge center is required to drive a given RF current through the bulk (equation (8)). The times of strongest current density in the bulk agree with the times of strongest electron heating rate such as shown in the right plot of figure 1 and in figure 3 for a CF_4 discharge at 50 Pa. The top plot of figure 5 shows the spatial profile of the reduced electric field at the time of maximum electron heating/current also for the two pressures investigated in CF_4 discharges at $\theta = 0°$ (30 Pa—$t \approx 11$ ns: blue dashed line, 50 Pa—$t \approx 16$ ns: red dotted line). In these strongly electronegative discharges, the reduced electric field in the bulk is approximately 200–250 Td, which is high enough to cause significant ionization [89, 90]. Consequently, the electron heating in the bulk increases significantly (figure 3) resulting in a high mean electron energy (figure 6) and ionization (figure 4) in the discharge center. The local extrema of the reduced electric field at the sheath edges coincide with the local extrema of the electron density at these times within one lf period, which changes the local conductivity and electric field (equation (8)). Under certain conditions, the total electron heating in the bulk exceeds the total sheath heating and the discharge is operated in the bulk heating mode. Such a scenario is observed at 50 Pa and $\phi_{lf} = \phi_{hf} = 50$ V in CF_4. At 30 Pa ($\phi_{lf} = \phi_{hf} = 100$ V), the reduced electric field in the bulk is similar and the total electron heating rate in the bulk is even slightly higher compared with the 50 Pa case. However, at 30 Pa the maximum sheath width is bigger compared with the 50 Pa case due to the higher driving voltage amplitude at similar positive ion densities. Thus, the sheath expansion heating is higher at 30 Pa compared with 50 Pa and the discharge is operated in a hybrid mode, where the sheath expansion heating is stronger than the bulk heating, but both contribute to the ionization.

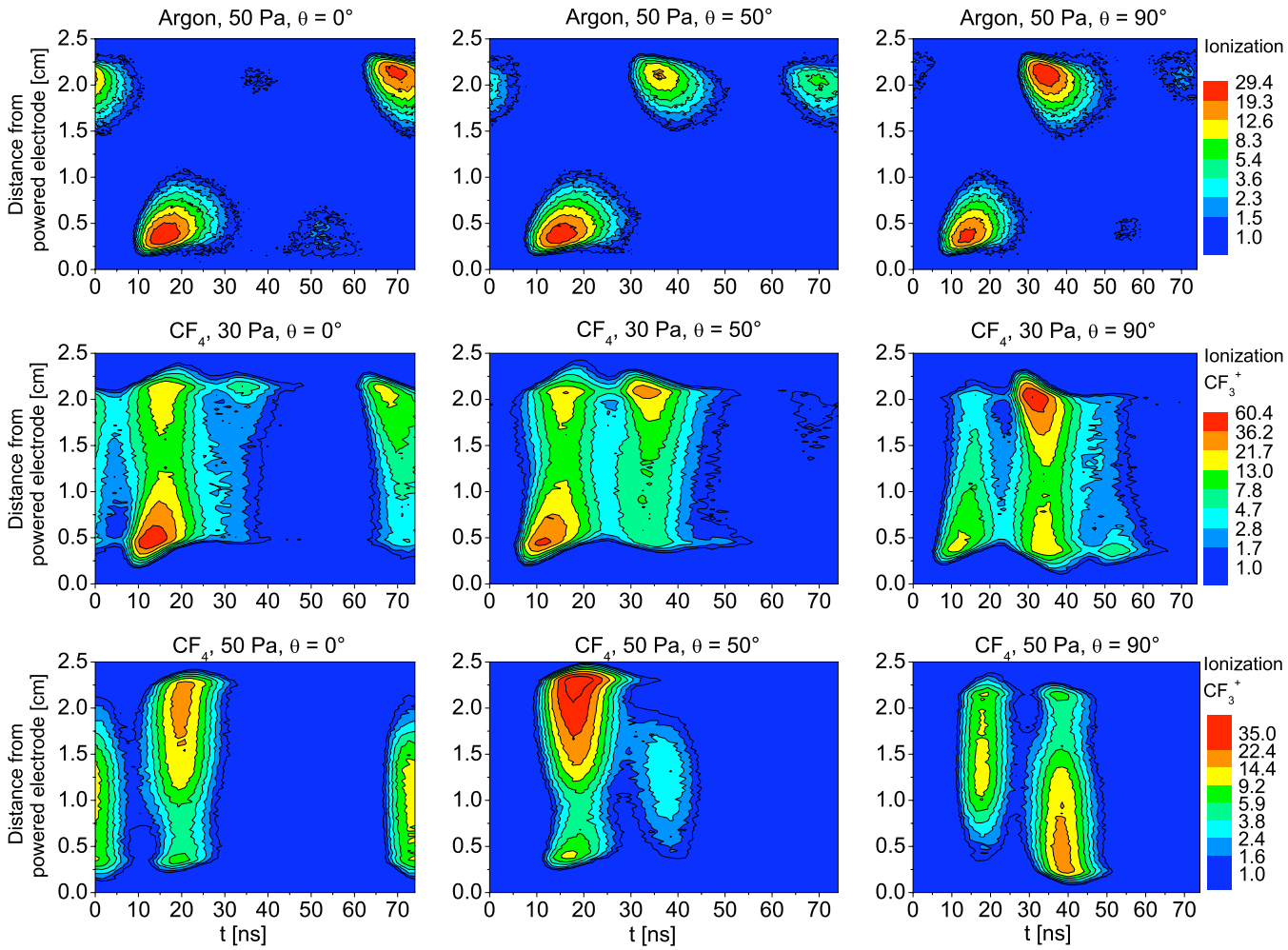

Figure 4. Spatio-temporal distribution of the ionization rate (generation of Ar^+/CF_3^+) in df discharges operated at 13.56 MHz + 27.12 MHz for different values of θ. First row: Ar, 50 Pa, $\phi_{lf} = \phi_{hf} = 50$ V. Second row: CF_4, 30 Pa, $\phi_{lf} = \phi_{hf} = 100$ V. Third row: CF_4, 50 Pa, $\phi_{lf} = \phi_{hf} = 50$ V. The color scale is given in 10^{20} m^{-3} s^{-1} and is the same for all plots in each row.

Generally, these results agree qualitatively with previous time averaged results of simulation studies of single frequency CF_4 discharges [30]. Our time resolved investigations provide a more detailed understanding of this bulk heating mode and aid the understanding of the transition from α-mode to the bulk heating mode. Proshina *et al* [30] found that, for a given driving voltage, the discharge will jump from α-mode operation into the bulk heating mode if the pressure is increased. This is caused by the increased electron attachment at higher pressures that causes a higher electronegativity and leads to a higher bulk electric field, which finally leads to enhanced ionization in the bulk. They also found that for a given pressure the discharge will jump from the bulk heating into α-mode, if the voltage is increased. This is caused by an increase in the sheath expansion heating relative to the bulk heating as a function of the driving voltage.

If the phase shift, θ, is changed, the applied voltage waveform and the RF current dynamics will change such as shown in figure 1. For any value of θ, the time average of the RF current vanishes. However, its dynamics and, therefore, the spatio-temporal electron heating and ionization rates depend on θ. At $\theta = 90°$, the role of both electrodes is reversed compared with $\theta = 0°$ and the electron heating and ionization dynamics change correspondingly (figures 3 and 4). At $\theta = 0°, 90°$, the RF current (figure 1 for CF_4 at 50 Pa) has one global maximum and one minimum within one lf period, whose absolute values are approximately the same. Thus, the electron heating has two similarly strong maxima within one lf period, which cause significant ionization. In electronegative CF_4 discharges, the bulk electric field is high at these times, but has different signs due to the different signs of the RF current, i.e. the bulk electrons are strongly accelerated toward the grounded and toward the powered electrode once per lf period, respectively (arrows in figure 3). At $\theta = 50°$, the RF current has one global maximum and two similarly strong minima, whose absolute values are lower than the global maximum. Thus, in CF_4 discharges at $\theta = 50°$, the bulk electric field, the electron heating and ionization rates are high only once per lf period, when electrons are strongly accelerated toward the grounded electrode. Under these conditions the absolute value of the bulk electric field increases toward the grounded electrode (middle plot in figure 5) due to the decreasing electron density (figure 2, equation (8)) at the time of maximum heating. This results in a maximum of the electron heating and ionization rates close to the sheath edge adjacent to the grounded electrode. At the two times within each lf period,

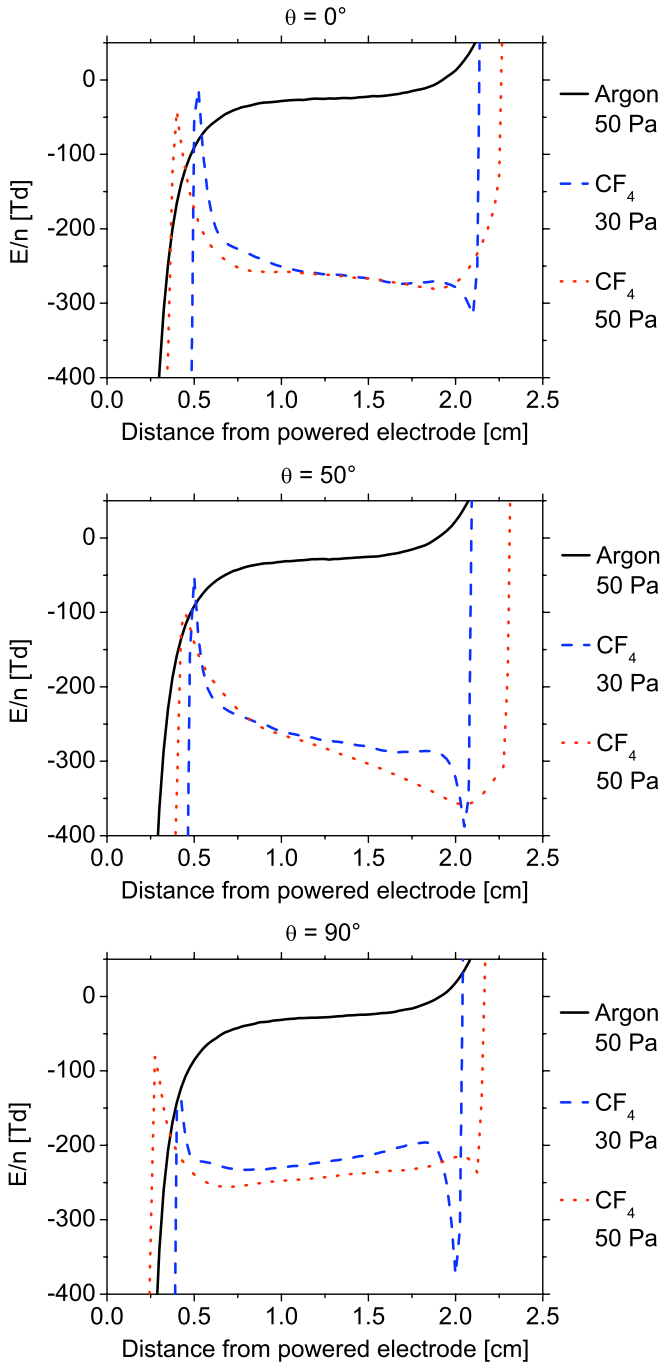

Figure 5. Spatial profile of the reduced electric field at the time of maximum electron heating (see figure 3) for different values of θ. The regions of strong electric field at the electrodes correspond to the boundary sheaths.

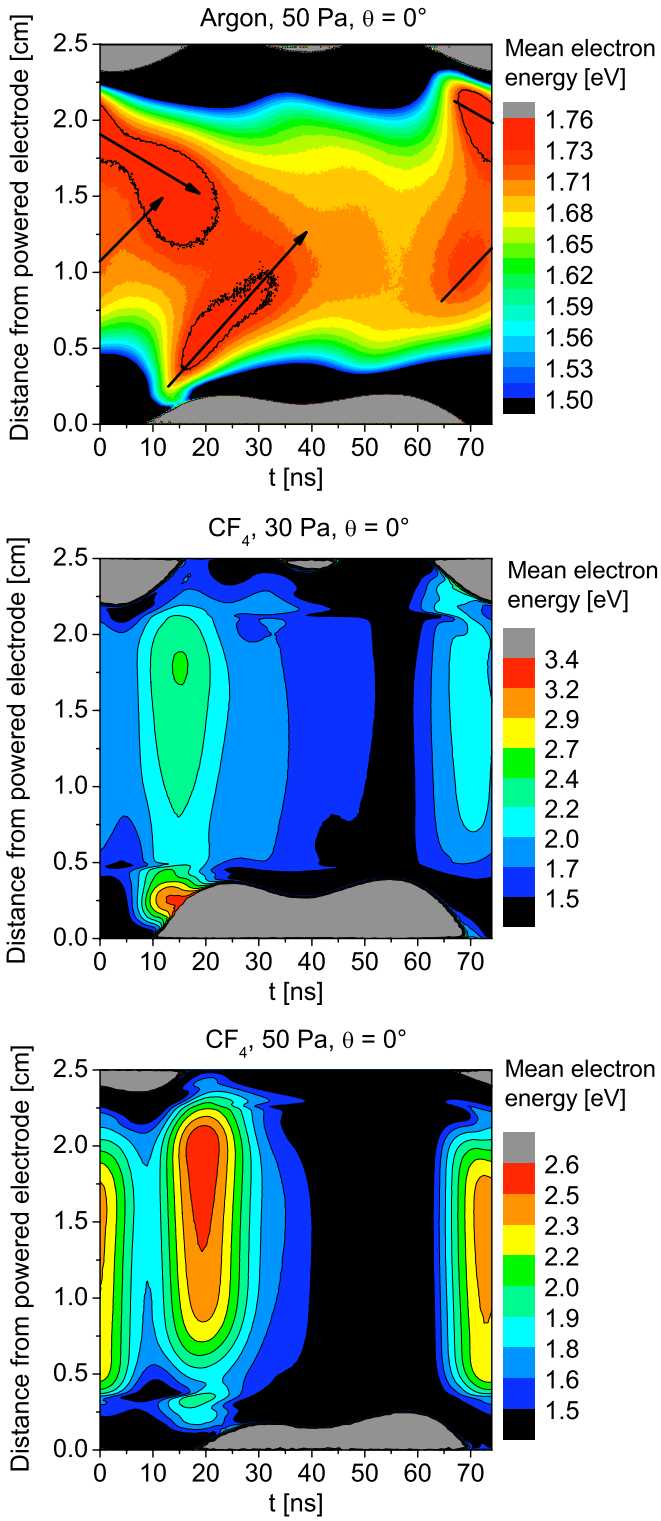

Figure 6. Spatio-temporal maps of the mean electron energy for $\theta = 0^\circ$ in df discharges operated at 13.56 MHz + 27.12 MHz. Top: Ar, 50 Pa, $\phi_{lf} = \phi_{hf} = 50$ V. Middle: CF_4, 30 Pa, $\phi_{lf} = \phi_{hf} = 100$ V. Bottom: CF_4, 50 Pa, $\phi_{lf} = \phi_{hf} = 50$ V. In the top plot, the arrows indicate the propagation of highly energetic electron beams. In the sheaths (gray areas), the mean electron energy is particularly high due to the presence of secondary electrons.

when the RF current is minimum, the bulk electric field and the electron heating rate have a local maximum, which is much lower than the global maximum. At these times electrons are accelerated toward the powered electrode such as indicated by the arrows in figure 3. At 50 Pa in CF_4, the reduced electric field in the bulk is too low to cause significant ionization in the bulk at these two times. This results in the asymmetric spatio-temporal ionization rate as shown in figure 4 (third row, second column), which shows one strong ionization source close to the grounded electrode. This causes the maxima of the ion density profiles to be shifted towards the grounded electrode (figure 2, third row, second column).

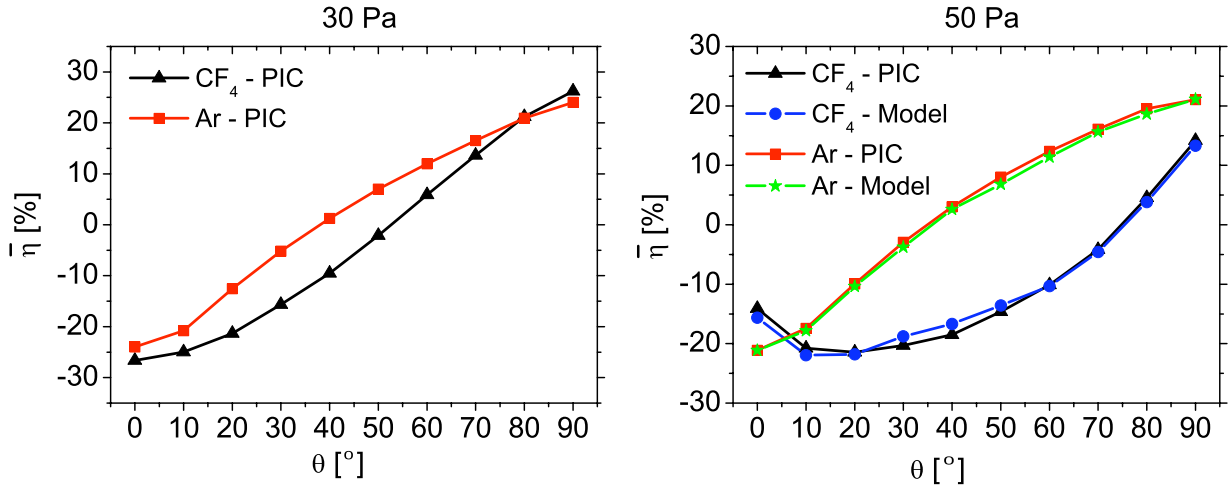

Figure 7. $\bar{\eta}$ as a function of θ in argon and CF_4 discharges at 30 Pa ($\phi_{lf} = \phi_{hf} = 100$ V, simulation results) and 50 Pa ($\phi_{lf} = \phi_{hf} = 50$ V, simulation and model results). For the model calculations, all terms of equation (3) are taken into account for CF_4 and only the first term is used for argon discharges.

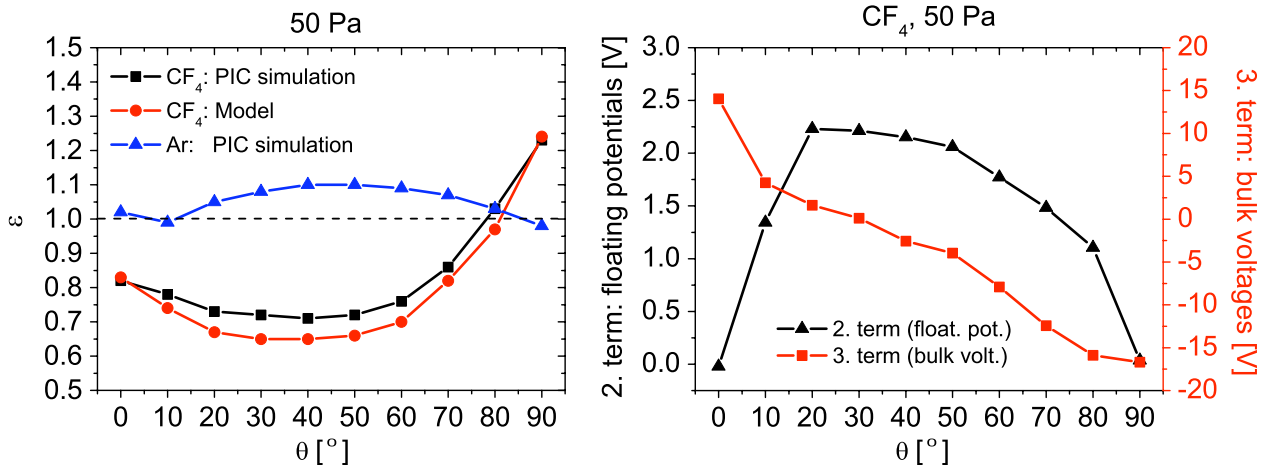

Figure 8. Left: symmetry parameter as a function of θ for argon and CF_4 discharges at 50 Pa ($\phi_{lf} = \phi_{hf} = 50$ V) resulting from the simulation and from a model for CF_4 assuming $\varepsilon = \bar{n}_{sp}/\bar{n}_{sg}$. Right: second and third terms of equation (3) as a function of θ in a CF_4 discharge at 50 Pa.

Finally, we tested the sensitivity of our simulation results on the ion–ion recombination rate coefficient for $\theta = 0°$. In the literature different values can be found (table 3, [24, 29, 30, 86, 87]) ranging from 1×10^{-13} to 5.5×10^{-13} m^3 s^{-1}. We use the value of 1×10^{-13} m^3 s^{-1} to ensure consistency with previous simulations [28]. If this rate coefficient is increased to 5.5×10^{-13} m^3 s^{-1}, we observe a decrease in the ion densities by a factor of approximately 2.5, while the electron density decreases only slightly by a factor of approximately 1.1. Thus, the electronegativity will be significantly lower if the higher rate coefficient is used. However, the spatio-temporal plots of the electron heating and ionization rates remain qualitatively unchanged, so that the presence and mechanisms of the bulk heating mode do not noticeably depend on this input parameter.

4.2. The EAE in df CF_4 discharges

Figure 7 shows simulation and model results for the dc self-bias normalized by the total amplitude of the driving voltage waveform, $\bar{\eta} = \eta/(\phi_{lf} + \phi_{hf})$, as a function of θ in electrically asymmetric CF_4 df discharges at 30 Pa ($\phi_{lf} = \phi_{hf} = 100$ V) and 50 Pa ($\phi_{lf} = \phi_{hf} = 50$ V). The results are compared with argon discharges under the same conditions. Similar to electropositive argon plasmas [65, 66, 68] a dc self-bias is generated electrically and can be tuned over a wide range by adjusting θ between 0° and 90°. These results demonstrate for the first time that the EAE also works in highly electronegative reactive CF_4 discharges. However, the dependence of $\bar{\eta}$ on θ is different compared with argon discharges, where $\bar{\eta}$ increases almost linearly as a function of θ. This difference is small at lower pressures of 30 Pa, where the discharge is operated in a hybrid mode, where sheath and bulk heating both contribute to the electron heating (figure 3), and increases significantly at higher pressures of 50 Pa, where the discharge is operated in the bulk heating mode. In this sense the EAE works differently in CF_4 compared with argon discharges.

This difference can be understood by the analytical model of the EAE [65, 76], which allows us to calculate $\bar{\eta}$ according to equation (3). The right plot of figure 7 shows model calculations of $\bar{\eta}$ as a function of θ for argon and CF_4 discharges

at 50 Pa using ε, ϕ^{f}_{sp}, ϕ^{f}_{sg}, ϕ^{b}_{max} and ϕ^{b}_{min} from the simulation. For the calculations in CF_4 discharges, all terms of equation (3) have to be taken into account, while using only the first term for argon plasmas is already sufficient. ε resulting from the simulation is shown as a function of θ in the left plot of figure 8 at 50 Pa. This plot also includes a calculation of ε based on the assumption $\varepsilon = \bar{n}_{sp}/\bar{n}_{sg}$ (equation (4)) for CF_4 discharges at 50 Pa (red line and dots). Obviously, the dependence of ε on θ is significantly different in CF_4 compared with argon discharges and finally causes the different dependence of $\bar{\eta}$ on θ. The calculation using $\bar{n}_{sp}$, $\bar{n}_{sg}$ from the simulation reproduces the symmetry parameter from the simulation well. Small differences are caused by the assumption of $(Q_{mg}/Q_{mp})^2 \cdot I_{sg}/I_{sp} = 1$ (equation (4)). This result shows that the main reason for the different dependence of ε and $\bar{\eta}$ on θ in CF_4 compared with argon is the difference between the mean effective ion densities in both sheaths. At values of θ around 0° and 90° this can be explained by the lower collisionality of the sheaths in CF_4 discharges at a given pressure due to the absence of symmetric charge exchange collisions. Thus, a finite bias, i.e. different mean sheath voltages, will cause different effective mean ion densities in both sheaths due to ion flux continuity in the sheaths. This mechanism is similar to the self-amplification of the EAE in argon discharges at lower pressures [65]. At values of θ around 45°, the bulk heating causes $\bar{n}_{sg}$ to increase relative to $\bar{n}_{sp}$ in CF_4 discharges at 50 Pa, which results in a decrease of the symmetry parameter (figure 8). As discussed in the previous section, for these phase angles the bulk heating causes an asymmetric spatio-temporal ionization rate with the main ionization source at the sheath edge adjacent to the grounded electrode (figure 4) and leads to shifted peaks of the ion density profiles (figure 2). This leads to different effective mean ion densities in both sheaths and causes the EAE to work differently in electronegative CF_4 discharges compared with electropositive argon discharges. This is an effect purely restricted to strongly electronegative discharges. This effect is more pronounced at 50 Pa, since the discharge is operated in the bulk heating mode, while it is operated in a hybrid mode at 30 Pa.

The small increase in ε in argon at 50 Pa for values of θ around 45° is caused by a similar mechanism: at these phase angles α-mode heating causes an asymmetric spatio-temporal ionization dynamics (figure 4). In contrast to CF_4 discharges, the main ionization source is located at the sheath edge adjacent to the powered electrode. However, the difference between the ionization maxima at both electrodes is much smaller compared with CF_4, and thus the asymmetry is much less pronounced. Nevertheless, this small asymmetry causes $\bar{n}_{sp}$ to be higher than $\bar{n}_{sg}$ and causes ε to be higher than unity at these phase angles.

The strong electronegativity of CF_4 discharges additionally affects the electrical bias generation directly via the high voltage drops across the bulk. The right plot of figure 8 shows the second and third terms of equation (3) as a function of θ for CF_4 discharges at 50 Pa, i.e. the effect of the bulk voltages at the times of maximum and minimum driving voltage and the floating potentials on the self-bias. The contribution of the bulk voltages decreases almost linearly as a function of θ, while the contribution of the floating potential is maximum at values of θ between 0° and 90°. The effect of the bulk voltages is higher compared with the floating potentials for most values of θ. The linear dependence of the bulk term on θ is the result of the complex dependence of ε on θ (figure 8) and different values of ϕ^{b}_{max} and ϕ^{b}_{min} depending on θ and the RF current at the time of maximum and minimum applied voltage. The bulk voltages cause $|\bar{\eta}|$ to decrease compared with electropositive discharges, where $\phi^{b}_{max} \approx \phi^{b}_{min} \approx 0$ V. In comparison with argon discharges under the same conditions, this effect compensates the self-amplification of the EAE in CF_4 due to the lower collisionality of the sheaths and leads to similar values of $\bar{\eta}$ at 0° and 90°, respectively (figure 7). The dependence of the floating potential term on θ is also a result of the bulk heating mode, which leads to a strong acceleration of electrons toward the grounded electrode at the time of sheath collapse at this electrode (figure 4) for values of θ between 0° and 90°. At these intermediate phase shifts the grounded electrode is bombarded by highly energetic electrons, which leads to an increase in ϕ^{f}_{sg} relative to $|\phi^{f}_{sp}|$. In combination with the dependence of ε on θ (left plot of figure 8) this effect leads to the behavior of the floating potential term as a function of θ shown in the right plot of figure 8.

In argon discharges under the same conditions, the second and third terms of equation (3) are essentially zero and $\bar{\eta}$ can be described correctly using only the first term such as shown in the right plot of figure 7. Thus, the effect of the bulk voltages and the floating potentials are characteristic for electronegative discharges.

Figures 9 and 10 show the ion flux energy distribution functions in argon and CF_4 discharges at 30 Pa ($\phi_{lf} = \phi_{hf} =$ 100 V) and 50 Pa ($\phi_{lf} = \phi_{hf} =$ 50 V) for different values of θ. Similar to electropositive argon discharges, the electrical generation of a dc self-bias via the EAE allows us to control the distribution functions in an opposite way at the two electrodes. The shape of the distribution functions is different in argon and CF_4 under the same conditions, since the sheaths are less collisional in CF_4 due to the absence of symmetric charge exchange collisions.

Figure 11 shows the mean ion energy, $\langle E_{i,p}\rangle$ and $\langle E_{i,g}\rangle$, at the powered and grounded electrode, respectively, as a function of θ in argon and CF_4 df discharges at 30 Pa ($\phi_{lf} = \phi_{hf} =$ 100 V) and 50 Pa ($\phi_{lf} = \phi_{hf} =$ 50 V). Similar to argon discharges, the EAE allows us to control the mean ion energies by a factor of approximately 2 in df discharges. The values of the mean ion energies at the electrodes are higher in CF_4 compared with argon for a given set of discharge conditions, since the sheaths are less collisional in CF_4. At 50 Pa, the dependence of the mean ion energies on θ is different in CF_4 compared with argon due to the different dependence of $\bar{\eta}$ on θ (figure 7), which is caused by the bulk heating. It should be noted that the range of ion energy and bias control can be significantly enlarged by adding further consecutive harmonics to the driving voltage waveform in argon discharges [75]. A similar effect is expected also in electronegative discharges. A verification of this hypothesis, however, remains a topic for future investigations.

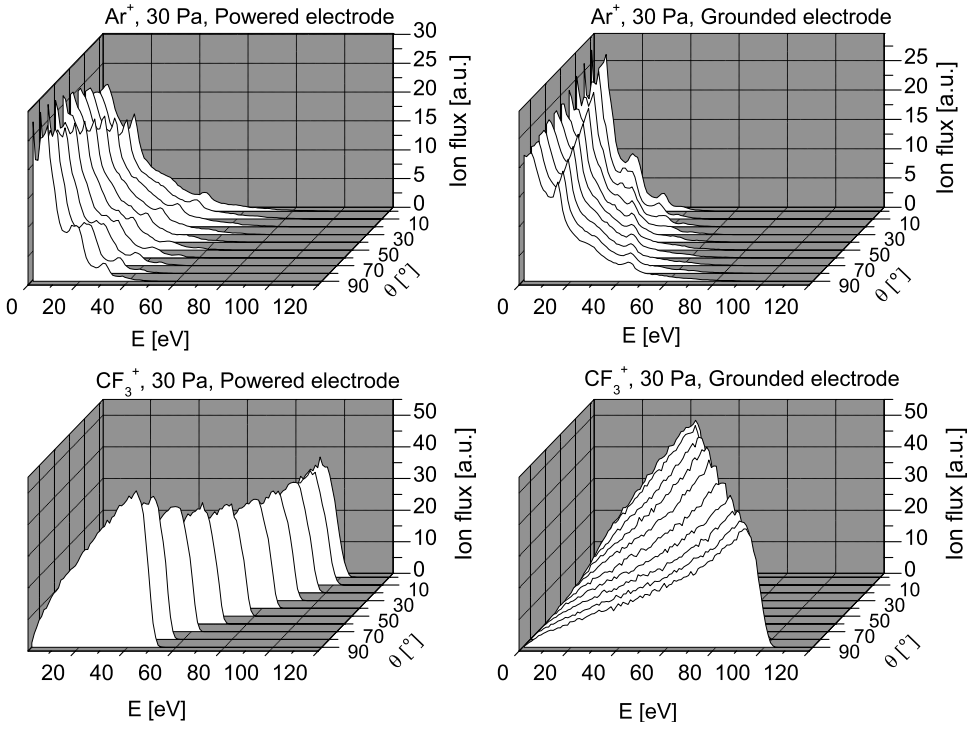

Figure 9. Ion flux energy distribution functions at both electrodes in argon and CF_4 df discharges operated at 30 Pa ($\phi_{lf} = \phi_{hf} = 100$ V) for different values of θ.

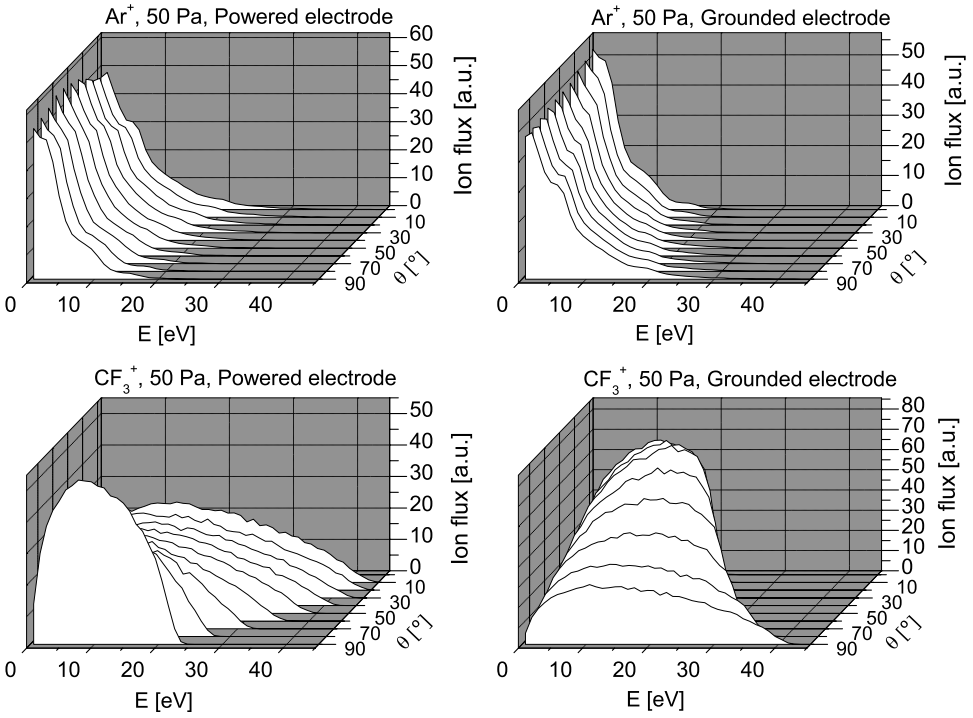

Figure 10. Ion flux energy distribution functions at both electrodes in argon and CF_4 df discharges operated at 50 Pa ($\phi_{lf} = \phi_{hf} = 50$ V) for different values of θ.

Figure 12 shows the ion flux, $\langle\Gamma_{i,p}\rangle$ and $\langle\Gamma_{i,g}\rangle$, at the powered and grounded electrode, respectively, as a function of θ in argon and CF_4 df discharges at 30 Pa ($\phi_{lf} = \phi_{hf} = 100$ V) and 50 Pa ($\phi_{lf} = \phi_{hf} = 50$ V). In argon discharges, the ion flux will change by a factor of maximum 1.35 at both electrodes, if θ is tuned from 0° to 90°, and the EAE allows an almost ideal separate control of ion energy and flux [66, 68]. In CF_4 discharges, the quality of this separate control via the EAE will be reduced if the discharge is operated in the bulk heating mode. At 50 Pa, we observe a change in the ion flux by a factor of

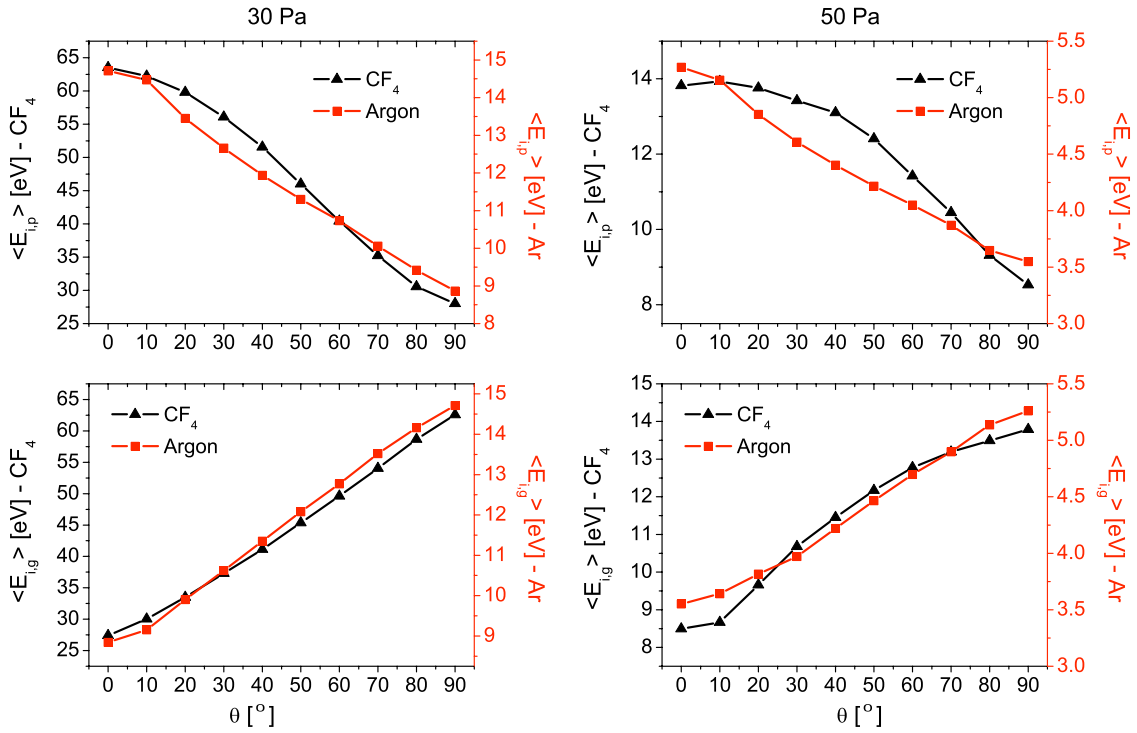

Figure 11. Mean ion energy at both electrodes as a function of θ in argon and CF_4 df discharges at 30 Pa ($\phi_{lf} = \phi_{hf} = 100$ V) and 50 Pa ($\phi_{lf} = \phi_{hf} = 50$ V).

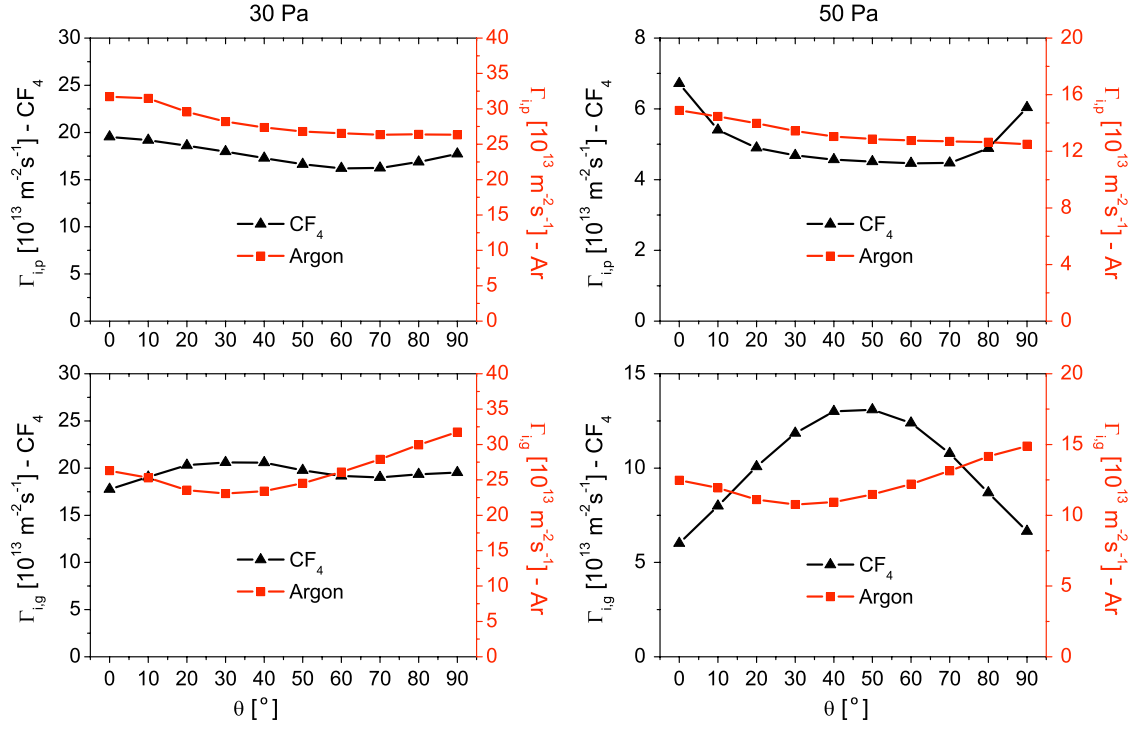

Figure 12. Ion flux at both electrodes as a function of θ in argon and CF_4 df discharges at 30 Pa ($\phi_{lf} = \phi_{hf} = 100$ V) and 50 Pa ($\phi_{lf} = \phi_{hf} = 50$ V).

maximum 1.5 at the powered electrode and 2.2 at the grounded electrode. This is caused by the bulk heating, which leads to an increased ionization source at the grounded electrode and a decreased ionization source at the powered electrode at values of θ around 45°.

5. Conclusions

We investigated the electron heating and the electrical asymmetry effect in dual-frequency capacitively coupled RF discharges operated in CF_4 at two consecutive harmonics

with fixed but adjustable phase shift, θ, between the driving frequencies by PIC/MCC simulations and the analytical model of the EAE. The results were compared with those obtained for argon discharges. Two different sets of discharge conditions at pressures of 30 and 50 Pa were analyzed for both gases.

The CF_4 discharges are found to be strongly electronegative with charged particle density profiles typical for electronegative discharges. The values of the charged particle densities and the electronegativity depend on the ion–ion recombination rate coefficient used in the simulation. The electronegativity increases as a function of pressure due to the enhanced electron attachment.

In contrast to electropositive argon discharges, which are operated in α-mode with maximum electron heating at the sheath edges, we observe the CF_4 discharges to be operated in a bulk heating mode at high pressures. In this mode, electrons are strongly heated in the plasma bulk by a high electric field, which is caused by the high electronegativity of the discharge leading to a low bulk conductivity. Thus, a high electric field is required to drive a given RF current through the bulk. In agreement with electron swarm studies, this field accelerates the bulk electrons to high energies, causes strong ionization in the bulk, and leads to spatio-temporal ionization dynamics different to classical capacitive RF discharges operated in α- or γ-mode. At lower pressures, we observe a hybrid mode, where α-mode and bulk heating both contribute to the heating dynamics.

If θ is tuned to values around 45°, the bulk heating will lead to asymmetric spatio-temporal ionization dynamics with one strong ionization source at the sheath edge adjacent to the grounded electrode due to a change in the driving voltage waveform. This asymmetry of the ionization rate causes the maxima of the ion density profiles to be shifted toward the grounded electrode. For the same reason, the ion flux to this electrode and the mean ion density within this sheath relative to the sheath at the powered electrode are increased, i.e. the discharge symmetry is changed.

This effect and the high voltage drop across the plasma bulk itself are found to affect the electrical generation of a dc self-bias via the EAE in CF_4 discharges in contrast to argon discharges. Both mechanisms are described and explained by the analytical model of the EAE. Generally, the EAE, i.e. the electrical generation of a dc self-bias as a function of θ, is found to work also in CF_4 discharges, but the functional dependence of the bias on θ is affected by the bulk heating of electrons. The quality of the separate control of the mean ion energy and flux at the electrodes via the EAE is reduced by the bulk heating via the asymmetric spatio-temporal ionization dynamics at values of θ around 45°.

Acknowledgments

This work has been funded by the Alexander von Humboldt foundation and the Hungarian Scientific Research Fund through grants OTKA-K-77653 and IN-85261. The authors thank U Czarnetzki, E Schüngel, R P Brinkmann and Z Lj Petrović for helpful discussions and their interest in this work. We thank V. Georgieva and A. Bogaerts for sharing their ion–molecule cross section set with us.

References

[1] Lieberman M A and Lichtenberg A J 2005 *Principles of Plasma Discharges and Materials Processing* 2nd edn (Hoboken, NJ: Wiley Interscience)
[2] Makabe T and Petrović Z Lj 2006 *Plasma Electronics: Applications in Microelectronic Device Fabrication* (London: Taylor and Francis)
[3] Lieberman M A 1988 *IEEE Trans. Plasma Sci.* **16** 638
[4] Lieberman M A and Godyak V A 1998 *IEEE Trans. Plasma Sci.* **26** 955
[5] Surendra M and Graves D B 1991 *Phys. Rev. Lett.* **66** 1469
[6] Turner M M 1995 *Phys. Rev. Lett.* **75** 1312
[7] Gozadinos G, Turner M M and Vender D 2001 *Phys. Rev. Lett.* **87** 135004
[8] Kaganovich I D 2002 *Phys. Rev. Lett.* **89** 265006
[9] Kaganovich I D, Polomarov O V and Theodosioue C E 2006 *IEEE Trans. Plasma Sci.* **34** 696
[10] Gans T, Schulz-von der Gathen V and Döbele H F 2004 *Europhys. Lett.* **66** 232
[11] Mussenbrock T and Brinkmann R P 2006 *Appl. Phys. Lett.* **88** 151503
[12] Mussenbrock T, Brinkmann R P, Lieberman M A, Lichtenberg A J and Kawamura E 2008 *Phys. Rev. Lett.* **101** 085004
[13] Czarnetzki U, Mussenbrock T and Brinkmann R P 2006 *Phys. Plasmas* **13** 123503
[14] Ziegler D, Mussenbrock T and Brinkmann R P 2008 *Plasma Sources Sci. Technol.* **17** 045011
[15] Schulze J, Heil B G, Luggenhölscher D, Brinkmann R P and Czarnetzki U 2008 *J. Phys. D: Appl. Phys.* **41** 195212
[16] Turner M M 2009 *J. Phys. D: Appl. Phys.* **42** 194008
[17] Belenguer Ph and Boeuf J P 1990 *Phys. Rev.* A **41** 4447
[18] Vender D and Boswell R 1992 *J. Vac. Sci. Technol.* A **10** 1331
[19] Schulze J, Heil B G, Luggenhölscher D, Mussenbrock T, Brinkmann R P and Czarnetzki U 2008 *J. Phys. D: Appl. Phys.* **41** 042003
[20] Sato A H and Lieberman M A 1990 *J. Appl. Phys.* **68** 6117
[21] Turner M M and Hopkins M B 1992 *Phys. Rev. Lett.* **69** 3511
[22] Czarnetzki U, Luggenhölscher D and Döbele H F 1999 *Plasma Sources Sci. Technol.* **8** 230
[23] Schulze J, Donkó Z, Heil B G, Luggenhölscher D, Mussenbrock T, Brinkmann R P and Czarnetzki U 2008 *J. Phys. D: Appl. Phys.* **41** 105214
[24] Georgieva V, Bogaerts A and Gijbels R 2003 *J. Appl. Phys.* **93** 2369
[25] Georgieva V, Bogaerts A and Gijbels R 2004 *Phys. Rev.* E **69** 026406
[26] Georgieva V and Bogaerts A 2005 *J. Appl. Phys.* **98** 023308
[27] Georgieva V and Bogaerts A 2006 *Plasma Sources Sci. Technol.* **15** 368
[28] Donkó Z and Petrović Z Lj 2006 *Japan. J. Appl. Phys.* **45** 8151
[29] Denpoh K and Nanbu K 1998 *J. Vac. Sci. Technol.* A **16** 1201
[30] Proshina O V, Rakhimova T V, Rakhimov A T and Voloshin D G 2010 *Plasma Sources Sci. Technol.* **19** 065013
[31] Denpoh K and Nanbu K 2000 *Japan. J. Appl. Phys.* **39** 2804
[32] Edelson D and Flamm D L 1984 *J. Appl. Phys.* **56** 1522
[33] Sobolewski M A, Wang Y and Goyette A 2002 *J. Appl. Phys.* **91** 6303
[34] Snijkers R J M M, van Sambeek M J M, Hoppenbrouwers M B, Kroesen G M W and de Hoog F J 1996 *J. Appl. Phys.* **79** 8982
[35] Haverlag M, Kono A, Passchier D, Kroesen G M W, Goedheer W J and de Hoog F J 1991 *J. Appl. Phys.* **70** 3472
[36] Booth J P, Corr C S, Curley G A, Jolly J, Guillon J and Foldes T 2006 *Appl. Phys. Lett.* **88** 151502
[37] Cunge G, Chabert P and Booth J P 2001 *J. Appl. Phys.* **89** 7750
[38] Booth J P 1999 *Plasma Sources Sci. Technol.* **8** 249
[39] Cunge G and Booth J P 1999 *J. Appl. Phys.* **85** 3952

[40] Booth J P, Cunge G, Chabert P and Sadeghi N 1999 *J. Appl. Phys.* **85** 3097
[41] Yan M, Bogaerts A, Goedheer W J and Gijbels R 2000 *Plasma Sources Sci. Technol.* **9** 583
[42] Gogolides E and Sawin H H 1992 *J. Appl. Phys.* **72** 3971
[43] Jiang W, Xu X, Dai Z-L and Wang Y-N 2008 *Phys. Plasmas* **15** 033502
[44] Kawamura E, Lichtenberg A J and Lieberman M A 2008 *Plasma Sources Sci. Technol.* **17** 045002
[45] Wang S-B and Wendt A E 2000 *J. Appl. Phys.* **88** 643
[46] Patterson M M, Chu H Y and Wendt A E 2007 *Plasma Sources Sci. Technol.* **16** 257
[47] Qin X V, Ting Y-H and Wendt A E 2010 *Plasma Sources Sci. Technol.* **19** 065014
[48] Rauf S and Kushner M J 1999 *IEEE Trans. Plasma Sci.* **27** 1329
[49] Dudin S V, Zykov A V, Polozhii K I and Farenik V I 1998 *Tech. Phys. Lett.* **24** 881
[50] Boyle P C, Ellingboe A R and Turner M M 2004 *Plasma Sources Sci. Technol.* **13** 493–503
[51] Boyle P C, Ellingboe A R and Turner M M 2004 *J. Phys. D.: Appl. Phys.* **37** 697
[52] Kitajima T, Takeo Y, Petrovic Z L and Makabe T 2000 *Appl. Phys. Lett.* **77** 489
[53] Denda T, Miyoshi Y, Komukai Y, Goto T, Petrovic Z L and Makabe T 2004 *J. Appl. Phys.* **95** 870
[54] Lee J K, Manuilenko O V, Babaeva N Yu, Kim H C and Shon J W 2005 *Plasma Sources Sci. Technol.* **14** 89
[55] Schulze J, Gans T, O'Connell D, Czarnetzki U, Ellingboe A R and Turner M M 2007 *J. Phys. D: Appl. Phys.* **40** 7008
[56] Gans T, Schulze J, O'Connell D, Czarnetzki U, Faulkner R, Ellingboe A R and Turner M M 2006 *Appl. Phys. Lett.* **89** 261502
[57] Schulze J, Donkó Z, Luggenhölscher D and Czarnetzki U 2009 *Plasma Sources Sci. Technol.* **18** 034011
[58] Turner M M and Chabert P 2006 *Phys. Rev. Lett.* **96** 205001
[59] Waskoenig J and Gans T 2010 *Appl. Phys. Lett.* **96** 181501
[60] Donkó Z *Proc. Symp. Application of Plasma Processes* ed J Matuska *et al* (*Podbanske Slovakia, 20–25 January 2007*) IL02 pp 21–4
[61] Donkó Z, Schulze J, Hartmann P, Korolov I, Czarnetzki U and Schüngel E 2010 *Appl. Phys. Lett.* **97** 081501
[62] Booth J P, Curley G, Marić D and Chabert P 2010 *Plasma Sources Sci. Technol.* **19** 015005
[63] Schulze J, Donkó Z, Schüngel E and Czarnetzki U 2011 *Plasma Sources Sci. Technol.* **20** 045007
[64] Heil B G, Schulze J, Mussenbrock T, Brinkmann R P and Czarnetzki U 2008 *IEEE Trans. Plasma Sci.* **36** 1404
[65] Heil B G, Czarnetzki U, Brinkmann R P and Mussenbrock T 2008 *J. Phys. D: Appl. Phys.* **41** 165202
[66] Donkó Z, Schulze J, Heil B G and Czarnetzki U 2008 *J. Phys. D: Appl. Phys.* **42** 025205
[67] Czarnetzki U, Heil B G, Schulze J, Donkó Z, Mussenbrock T and Brinkmann R P 2009 *J. Phys. Conf. Ser.* **162** 012010
[68] Schulze J, Schüngel E, Donkó Z and Czarnetzki U 2009 *J. Phys. D: Appl. Phys.* **42** 092005
[69] Donkó Z, Schulze J, Czarnetzki U and Luggenhölscher D 2009 *Appl. Phys. Lett.* **94** 131501
[70] Longo S and Diomede P 2009 *Plasma Process. Polym.* **6** 370
[71] Schulze J, Schüngel E, Donkó Z and Czarnetzki U 2009 *J. Appl. Phys.* **106** 063307
[72] Schulze J, Schüngel E, Donkó Z and Czarnetzki U 2010 *Plasma Sources Sci. Technol.* **19** 045028
[73] Schulze J, Schüngel E, Donkó Z and Czarnetzki U 2010 *J. Phys. D: Appl. Phys.* **43** 225201
[74] Zhang Q-Z, Jiang W J, Hou L-J and Wang Y-N 2011 *J. Appl. Phys.* **109** 013308
[75] Schulze J, Schüngel E, Donkó Z and Czarnetzki U 2011 *Plasma Sources Sci. Technol.* **20** 015017
[76] Czarnetzki U, Schulze J, Schüngel E and Donkó Z 2011 *Plasma Sources Sci. Technol.* **20** 024010
[77] Kollath R 1956 *Encyclopedia of Physics* vol XXI, ed S Flügge (Berlin: Springer) p 264
[78] Phelps A V and Petrović Z Lj 1999 *Plasma Sources Sci. Technol.* **8** R21
[79] Phelps A V 1994 *J. Appl. Phys.* **76** 747
[80] Phelps A V http://jilawww.colorado.edu/∼avp/collision_data/ unpublished
[81] Kurihara M, Petrović Z Lj and Makabe T 2000 *J. Phys. D: Appl. Phys.* **33** 2146
Dujko S, Raspopović Z M and Petrović Z Lj 2005 *J. Phys. D: Appl. Phys.* **38** 2952
[82] Bonham R A 1994 *Japan. J. Appl. Phys.* **33** 4157
[83] Nanbu K 2000 *IEEE Trans. Plasma Sci.* **28** 971
[84] Nanbu K and Kitatani Y 1995 *J. Phys. D: Appl. Phys.* **28** 324
[85] Nanbu K and Denpoh K 1998 *J. Phys. Soc. Japan* **67** 1288
[86] Rauf S and Kushner M J 1997 *J. Appl. Phys.* **82** 2805
[87] So S-Y, Oda A, Sugawara H and Sakai Y 2002 *J. Phys. D: Appl. Phys.* **35** 2978
[88] Brinkmann R P 2007 *J. Appl. Phys.* **102** 093302
[89] SIGLO database http://www.lxcat.laplace.univ-tlse.fr retrieved 10 January 2011
[90] Hagelaar G J M and Pitchford L C 2005 *Plasma Sources Sci. Technol.* **14** 722